Journal of Materials Chemistry A

Accepted Manuscript

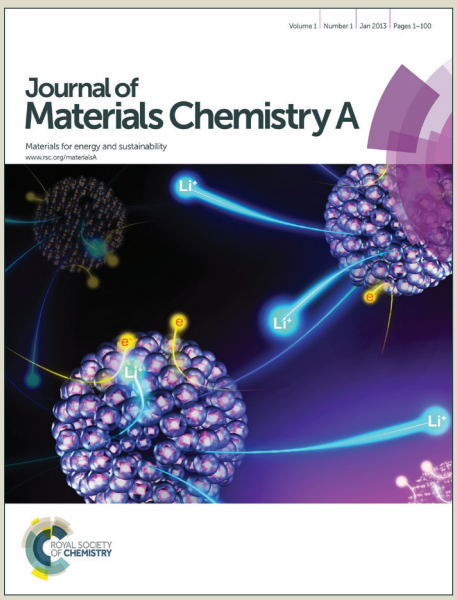

ROYAL SOCIETY OF CHEMISTRY

www.rsc.org/materialsA

Cite this: DOI: 10.1039/c0xx00000x

www.rsc.org/xxxxxx

ARTICLE TYPE

Facile fabrication and electrochemical performance of flower-like Fe_3O_4@C@layered double hydroxide (LDH) composite

Lei Li, Rumin Li,* Shili Gai, Fei He, and Piaoping Yang*

Received (in XXX, XXX) Xth XXXXXXXXX 20XX, Accepted Xth XXXXXXXXX 20XX

DOI: 10.1039/b000000x

In this paper, a novel core-shell structured Fe_3O_4@C@Ni-Al LDH composite containing carbon-coated Fe_3O_4 magnetic core and a layered double hydroxide (LDH) had been successfully prepared by a combination of the hydrothermal method and a facile *in situ* growth process. The Fe_3O_4@C@Ni-Al LDH microspheres were characterized by X-ray diffraction (XRD), scanning and transmission electron microscopy (SEM and TEM), high-resolution transmission electron microscopy (HRTEM), Fourier transformed infrared (FT-IR), X-ray photoelectron spectra (XPS), and N_2 adsorption/desorption methods. Owing to the unique layered feature, the composite displays core-shell structure with flower-like morphology, ultra high surface area (792 m^2/g) and specific pore size distribution. Moreover, the as-synthesized Fe_3O_4@C@Ni-Al LDH microsphere as an electrode material was fabricated into a supercapacitor and characterized by cyclic voltammetry (CV), electrochemical impedance spectroscopy (EIS), and galvanostatic charge-discharge measurements. It turned out that the Fe_3O_4@C@Ni-Al LDH exhibits specific capacitance of 767.6 F/g, good rate capability, and remarkable cycling stability (92% after 1000 cycling). Therefore, such novel synthetic route to assemble the high-performance electrochemical capacitor may open a new strategy to prepare other materials with largely enhanced electrochemical property, which can be of great promise in energy storage device applications.

1. Introduction

Considering the increasing energy and environmental demands, energy storage device with sustainable, renewable and efficient properties has become a pressingly essential need in both scientific and technological area.[1–5] Electrochemical capacitors (ECs, also known as supercapacitors or ultracapacitor), which are considered as a promising candidate to power the next generation of energy storage device,[6–8] have been widely investigated to meet the increasing requirements owing to their high power density, long cycling life and high rate capacity compared to secondary batteries.[9–11] On the basis of the energy storage mechanism, there are three major types of electrode materials reported for ECs: carbonaceous materials, metal oxides/hydroxides, and conduction polymers. Among them, transition metal oxides, the typical pseudocapacitive materials such as RuO_2,[12] Co_3O_4[13] and some kinds of amorphous hydrated,[14–16] have been explored to be excellent electrode because of their ideal pseudocapacitive behaviours and good reversibility. However, the applications have been hindered due to high costs and environmental toxicity. Thereby, it is obvious that alternative transition metal oxide with low cost, common and environmental properties is more suitable for the development of metal oxides/hydroxides supercapacitors.

As a kind of desirable pseudocapacitive material which has advantages of low cost, natural abundance and low environment impact, Fe_3O_4 has been extensively studied as alternative electrode material for supercapacitors.[17–21] It also has a relatively high theoretical Li storage capacity,[22,23] suggesting Fe_3O_4 can offer high pseudo charge capacitance through redox reaction. To extend the use of Fe_3O_4 in the area of electrochemistry, several techniques have been employed to prepare Fe_3O_4 with controlled morphologies and structures,[24–26] including electroplating,[27] hydrothermal,[20,28] the sol–gel route[17] and microwave method.[29] Nevertheless, low surface area and gravimetric capacitance of Fe_3O_4 particles, which results from its high material density and mild redox reaction with ions in electrolyte, restrict their application as electrode of supercapacitor.[17,30–32] Despite the disappointing gravimetric capacitance, Fe_3O_4 can be exploited with considerable areal capacitance through some surface modification and coating procedure to address the shortcomings mentioned above.

Carbon modifications, especially carbon coating process have been frequently employed in electrochemical capacitors.[33–35] Compared with composites incorporated with one-dimensional carbon nanotubes or carbon nanofibers, carbon-coating is facile, cost-effective and environment-friendly. Moreover, the advantages of high surface availability, good electrical conductivity and excellent chemical stability of carbon layer can significantly enhance the electronic conductivity of the electrode materials and increase the surface area of electrode so as to allow more sites for charge storage, which results in high electrochemical performance.[1, 36–39]

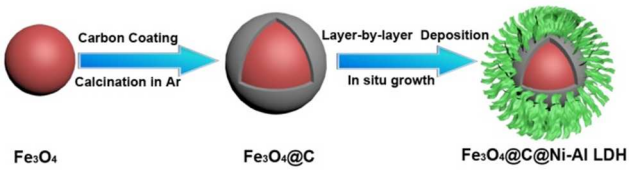

Scheme 1 Schematic illustration for preparation of Fe_3O_4@C@Ni-Al LDH microspheres.

Meanwhile, layered double hydroxides, especially Ni-Al LDH have been widely used in catalysis, anion exchange, acid absorbents, electrode for electrochemical sensors and alkaline secondary batteries due to their large-area uniform films.[40–44] The structure of Ni-Al LDH contains positively charged host layers with two kinds of metallic cations and exchangeable hydrated anions located in the interlayer gallery for charge balance. And Ni-Al LDH has been explored as electrode material of ECs due to its low cost, high pseudocapacitance, long cycle life and high oxidization potential.[45–48] The improvement of specific capacitance and high rate capability of Ni-Al LDH modificatory composites are mainly ascribed to the specific nanostructure with large surface area, which offers effective diffusion channels for the electrolyte ions (OH^-).[49–54] What's more, the abundant mesopores in Ni-Al LDH structure can act as an "ion reservoir", which guarantees a steady supply of OH^- ions as well as high current density of the faradic reaction for energy storage just like the carbon layer.[55–57] Therefore, it makes great significance for combining carbon coating layers and LDH to improve the electrochemical performance.

Motivated by the above analysis, we present a facile and efficient method to synthesize Fe_3O_4@C@Ni-Al LDH through carbon coating process and an *in situ* growth technique, which was depicted in Scheme 1. Fe_3O_4@C microspheres with good electrochemical property are prepared *via* hydrothermal reaction and subsequent calcination under high-purity Ar procedure. The modification of carbon layer plays an important role in the preparation of the sample and the connection between Fe_3O_4 and Ni-Al LDH for enhancing electrochemical property. On one hand, carbon layer can provide a support for anchoring LDH layer. On the other hand, porous carbon has excellent electrical conductivity and can offer better access for electrolyte into the entire structure. In the process of LDH coating, it is noteworthy that the use of *in situ* growth method enables LDH nanoplatelets to adhere on the surface of the Fe_3O_4@C core strongly, and the emerging of the mesopores on LDH surface can initiate a more reversible faradic redox reaction, which plays a key role in enhancing pseudocapacitance property. With the elegant combination of the carbon and Ni-Al LDH layers, the microspheres can not only improve the conductivity of Fe_3O_4, but also avoid the loss of cyclability during repetitive incorporation extraction processes. As a result, the Fe_3O_4@C@Ni-Al LDH composite gives a maximum specific capacitance of 767.6 F/g, much higher than that of pure Fe_3O_4 reported before. In addition, this composite exhibits high cycle performance and good rate capability. This novel modification route towards Fe_3O_4 is a convenient and potential way for producing a secondary emerging material, which is expected to be applicable in fabrication of other metal oxide supercapacitors materials.

2. Experimental section

2.1. Synthesis

Synthesis of Fe_3O_4 microspheres. The Fe_3O_4 microspheres were prepared according to the previous report.[58] Briefly, 2.70 g of $FeCl_3{\cdot}6H_2O$ and 7.20 g of sodium acetate were dissolved in 100 mL of ethylene glycol to form a clear solution under magnetic stirring. Afterwards, the mixture was stirred vigorously for 30 min, then sealed in a Teflon-lined stainless-steel autoclave and heated at 200 °C for 20 h. After the autoclave was cooling down to room temperature, the resulting black magnetite particles were washed several times with ethanol and dried in vacuum at 60 °C for 6 h.

Synthesis of Fe_3O_4@C microspheres. 0.2 g of magnetic microspheres was ultrasonicated for 10 min in 0.1 M HNO_3, followed by washing with deionized water. Then, the treated Fe_3O_4 microspheres were introduced in 0.5 M aqueous glucose solution and ultrasonicated for another 10 min. Then the resulting black suspension was transferred to autoclaves, kept at 190 °C for 12 h, and cooled to room temperature. The obtained microspheres were withdrew with the help of a magnet and washed with deionized water. After the mixture vacuum-dried at room temperature, a certain amount of as-obtained powder was loaded into a tube furnace and heated under high-purity Ar at 600 °C for 4 h.

Synthesis of Fe_3O_4@C@Ni-Al LDH microspheres. Fe_3O_4@C@AlOOH microspheres were formed through a layer-by-layer (LBL) deposition process. And the preparation of AlOOH primer sol by sol–gel method has been described previously.[40] Firstly, Fe_3O_4@C microspheres were dispersed in the AlOOH primer sol with vigorous agitation for 1.5 h. The obtained Fe_3O_4@C@AlOOH was withdrawn with a bar magnet and washed with ethanol. The resulting Fe_3O_4@C@AlOOH was dried in air for 30 min. The whole process (dispersion, withdrawing, and drying) was repeated ten times.

Subsequently, 0.01 mol of $Ni(NO_3)_2{\cdot}6H_2O$ and 0.015 mol of urea were dissolved in 70 mL of deionized water to form a solution. Fe_3O_4@C@AlOOH (0.2 g) was placed in the above solution in an autoclave at 100 °C for 48 h. Finally, the resulting Fe_3O_4@C@Ni-Al LDH microspheres were separated by a magnet, washed several times with ethanol, and dried in vacuum at 60 °C for 12 h.

2.2. Characterization

X-ray diffraction (XRD) was obtained in the 2θ range of 10–80°C using a Rigaku-Dmax 2500 diffractometer with Cu Kα radiation (λ = 0.15405 nm). The X-ray photoelectron spectra (XPS) were recording on a VG ESCALAB MK II electron energy spectrometer using Mg KR (1253.6 eV) as the X-ray excitation source. Fourier transform IR (FT-IR) spectra were measured on a PerkinElmer 580B IR spectrophotometer using KBr pellet technique. SEM images were obtained from a field emission scanning electron. TEM was carried out from a FEI Tecnai G^2 S-Twin transmission electron microscope with a field emission gun operating at 200 kV elucidate the dimensions and the structural details of the particles. N_2 adsorption/desorption isotherm was performed at 77 K using a Micromeritics Tristar 30s0M instrument. The specific surface areas were determined by the Brunauer-Emmett-Teller (BET) method and the pore size

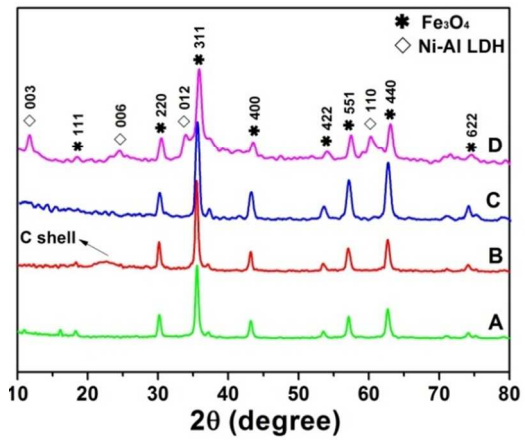

Fig. 1 XRD patterns of Fe_3O_4 (A), Fe_3O_4@C (B), Fe_3O_4@C@AlOOH (C) and Fe_3O_4@C@Ni-Al LDH (D).

distributions were calculated using Barret-Joyner-Halenda (BJH) method. All of the measurements were performed at room temperature.

2.3. Electrode preparation and electrochemical characterization

The as-prepared Fe_3O_4@C@Ni-Al LDH microspheres, acetylene black and polyvinylidene difluoride (PVDF) were mixed in a mass ratio of 80: 15: 5 and dispersed in ethanol to form slurry. Then the resulting mixture was coated on a piece of nickel foam current collector (1.0 cm × 1.0 cm) with a spatula, which was followed by drying at 90 °C for 12 h in a vacuum oven. Electrochemical measurements were conducted in a three-electrode arrangement in 6 M KOH electrolyte. A bright Pt plateand Hg/HgO electrode was used as the counter electrode and out on a CHI666D electrochemical workstation at room temperature.

3. Results and discussion

3.1. Material characterization

To clarify the structure of the composites, XRD experiments were carried out. Fig. 1 shows the XRD patterns of Fe_3O_4, Fe_3O_4@C, Fe_3O_4@C@AlOOH, and Fe_3O_4@C@Ni-Al LDH composite, respectively. The diffraction peaks in curve A can be indexed to cubic Fe_3O_4 phase (JCPDS No. 19–0629). After coating with carbon layer, the diffraction pattern shows that Fe_3O_4@C microspheres have similar diffraction peaks to those of Fe_3O_4 except for a weak broad peak assigned to amorphous carbon, suggesting that the magnetic cores are well retained in the carbon shell, which is accordance with the following TEM results (Fig. 3E). The XRD pattern of the Fe_3O_4@C@AlOOH microspheres is much similar to that of Fe_3O_4@C, showing the amorphous nature of the AlOOH coating. As for Fe_3O_4@C@Ni-Al LDH, besides the obvious diffraction peaks of Fe_3O_4 phase, the typical reflections of Ni-Al LDH phase (JCPDS No. 48–0593) marked with ◇ of (003), (006), (012), and (110) planes can be observed clearly. The obvious diffraction peaks of LDH material suggest the highly crystallinity and successful coating of Ni-Al LDH.

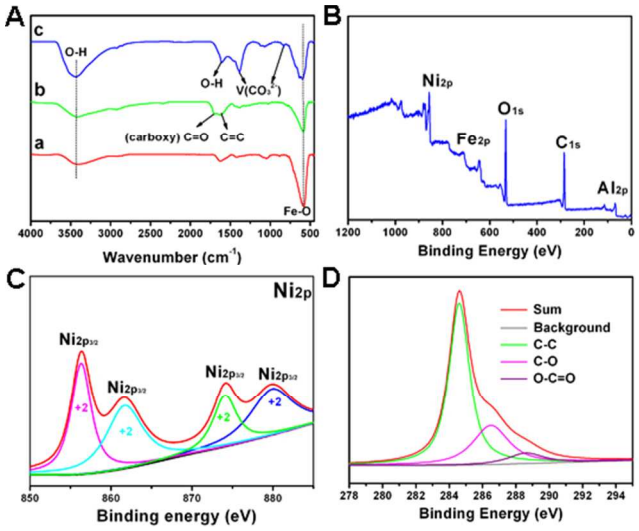

Fig. 2 FT-IR spectra (A) for Fe_3O_4 (a), Fe_3O_4@C (b), and Fe_3O_4@C@Ni-Al LDH composite (c); XPS survey spectrum (B), Ni 2p (C) and C 1s (D) spectra of Fe_3O_4@C@Ni-Al LDH composite.

Fig. 2A displays the FT-IR spectra of Fe_3O_4, Fe_3O_4@C and Fe_3O_4@C@Ni-Al LDH ranging from 4000 to 400 cm^{-1}. In the spectrum of Fe_3O_4 powder, a peak at 580 cm^{-1} is assigned to the Fe−O bond vibration. For Fe_3O_4@C in curve b, the bands C=O (carboxylic acid) at 1718 cm^{-1} and C=C at 1617 cm^{-1} are the characteristic features of graphite oxide, resulting from the carbonization of glucose during hydrothermal reaction and calcination process. After a LBL deposition process followed by an *in situ* growth technique, successful formation of Ni-Al LDH has been confirmed by the presence of the bands at 1389 and 831 cm^{-1}, which are the vibration of CO_3^{2-} corresponding to the interlayer anion of layered Ni-Al LDH. Meanwhile, the broad peak centred at 3469 cm^{-1} is attributed to the O–H stretching vibration of water molecules in the interlayer and hydrogen-bonded OH groups, accompanied with the bendingmode at 1611 cm^{-1}. In order to further characterize the formation of carbon and Ni-Al LDH layer, the composition of Fe_3O_4@C@Ni-Al LDH was analyzed by XPS. Fig. 2B displays the survey spectrum of Fe_3O_4@C@Ni-Al LDH, in which the peaks of Ni 2p (amplified lines in Fig. 2C) and Al 2p are obviously observed, suggesting

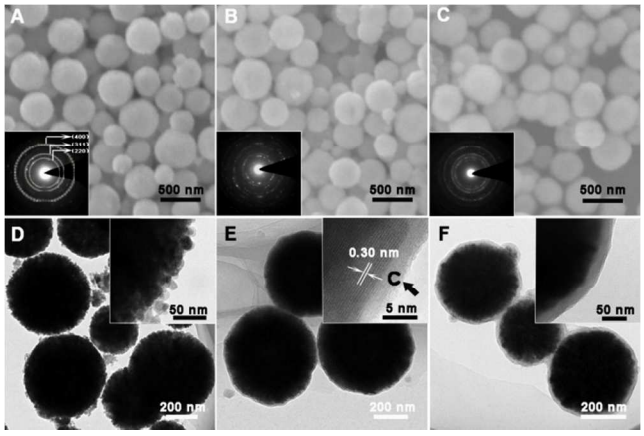

Fig. 3 SEM and TEM images of Fe_3O_4 (A, D), Fe_3O_4@C (B, E), Fe_3O_4@C@AlOOH composite (C, F). Insets are their corresponding SAED images and enlarged TEM images.

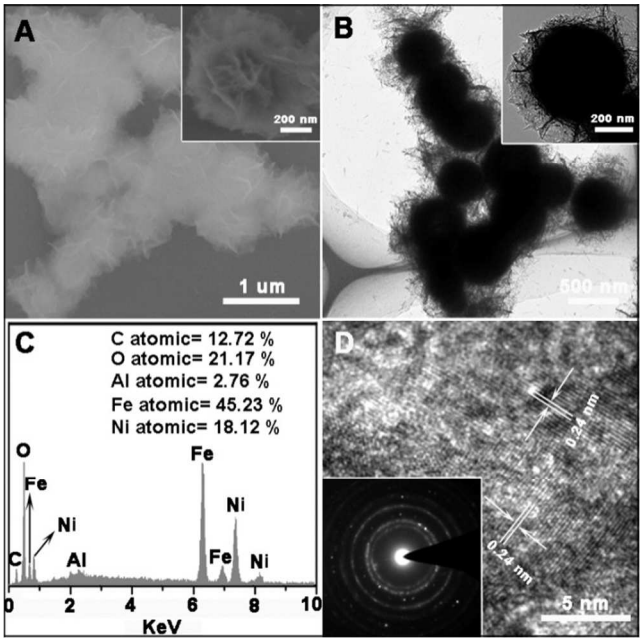

Fig. 4 SEM image (A), TEM image (B), EDS (c) and HRTEM image of Fe_3O_4@C@Ni-Al LDH composite. Insets in panel A, B and D are their corresponding enlarged images and SAED image.

the formation of Ni-Al LDH layer. From the fine spectrum of Ni 2p (Fig. 2c), the valence state of element Ni can be verified to be +2. By using a Gaussian fitting of the sp2 hybridised carbon atoms (C–C), which can further confirm the formation of carbon layer with graphite oxide character.[19,59] Fig. 3 display the respective SEM image of Fe_3O_4, Fe_3O_4@C and Fe_3O_4@C@AlOOH composites, which all exhibit a well-dispersed and near-spherical morphology without significant change, indicating the uniform outer coating layer. TEM image shows that the Fe_3O_4 particles possess a rough surface and have an average diameter of 350 nm (inset, Fig. 3D). After coating a carbon layer, the as-obtained Fe_3O_4@C microspheres exhibit a relative smooth surface with a thin layer about 3–5 nm (inset, Fig. 3E). The selected area electron diffraction (SAED) pattern (insets in Fig. 3A, B and C) reveals that these particles are magnetite Fe_3O_4 with a face-centered cubic crystal structure and carbon layer and AlOOH are amorphous. From the lattice fringes in the core is obvious, and the distance between adjacent lattice fringes (marked by the arrows) is 0.30 nm which is corresponding to the d_{220} spacing of cubic phased Fe_3O_4 (JCPDS No. 19–0629). The results provide the experimental proof that Fe_3O_4 core has successfully been encapsulated in the carbon shell. After further coating of AlOOH layer, the layer thickness of the as-prepared product is increased to 15 nm (inset, Fig. 3F), indicating the uniform coating after LBL deposition process.

The representative SEM image of as-prepared flower-like Fe_3O_4@C@Ni-Al LDH are shown in Fig. 4A. After an *in situ* growth reaction between AlOOH and Ni^{2+} salt, the surface of Fe_3O_4@C was coated by a uniform Ni-Al LDH shell. The high magnification image of an individual microsphere (inset, Fig. 4A) verifies that the flower-like LDH is self-assembled by small nanopetals. In the TEM image (Fig. 4B), a compact core and the exterior flower-like hierarchical microstructure demonstrate that Ni-Al LDH shell is composed of abundant randomly assembled

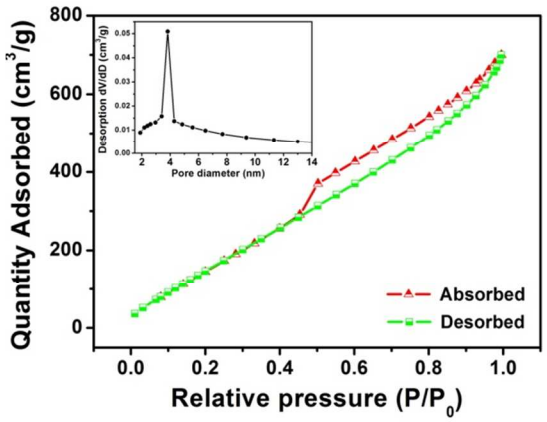

Fig. 5 N_2 sorption isotherms and pore size distribution (inset) of Fe_3O_4@C@Ni-Al LDH composite.

irregular-shaped nanopetals with a thickness of about 80 nm. And it makes more sense that the nanopetals are interconnected with each other, which is necessary to energy storage performance. On the one hand, the relative high density of center thereby ensures good electrical conductivity for updating electrochemical property. On the other hand, the unique loose feature of the Ni-Al LDH on the surface of Fe_3O_4@C can increase the external surface of the microspheres so as to make more electrical contact with the current collector, which is beneficial for higher charge transfer kinetics and an improvement of electrochemical capacity. The HRTEM image in Fig. 4D reveals the obvious lattice image obtained at the edge of the particle. The typical lattice fringe spacing is determined to be 0.24 nm, which is consistent with the (012) plane of a Ni-Al LDH phase. The selected area electron diffraction (SAED) pattern exibits obvious hexagonally arranged spots of Fe_3O_4, while the pattern of Ni-Al LDH can not be seen due to the low crystallinity compared to Fe_3O_4. In EDS spectrum, the existence of Fe, Al, Ni, C, and O elements can further confirm the formation of the carbon shell and Ni-Al LDH flowerlike nanopetals on Fe_3O_4@C microspheres. It is worth noting that the ratio of Ni and Al is 6.5 in Ni-Al LDH, which is consistent with the result calculated from XPS.

It is well-known that the surface area and pore-size distribution are two dominating factors for the electroactive materials to accommodate superficial electrochemical active sites and reduce the mass transfer in the Faradaic redox reactions. Herein, the as-prepared Fe_3O_4@C@Ni-Al LDH was further determined for the specific surface area and porosity by nitrogen sorption measurements. Fig. 5 displays the N_2 adsorption/desorption isotherm and the corresponding pore-size distribution curve (inset) for the sample. The synthetic microspheres display a typical IV isotherm, indicating the presence of mesopores. Moreover, the shape of hysteresis loops is H_3-type ($P/P_0 > 0.4$) and does not perform any limiting adsorption at high P/P_0 region, associated with aggregates of flower-like particles, giving rise to slit-like pores, which is well consistent with the SEM and TEM results. The pore-size distribution of the sample, derived from desorption data and calculated from the isotherm using the BJH model, exhibits unimodal porosity with an average of 4.0 nm, further confirming the existence of mesopores. Obviously, the measured pore size is within 2−5 nm, which is optimal for the behaviour of supercapacitors. The Brunauer-Emmett-Teller (BET) specific

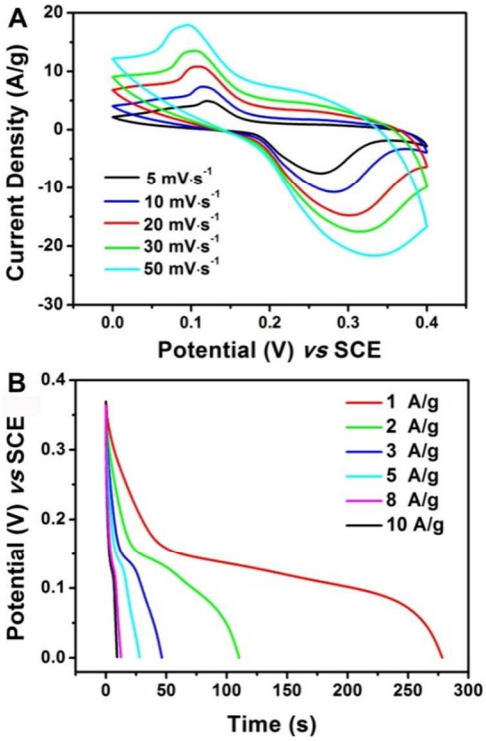

Fig. 6 Cyclic voltammograms (A) of Fe_3O_4@C@Ni-Al LDH electrodes measured at scan rates from 5–50 mV/s, discharge curves (B) of Fe_3O_4@C@Ni-Al LDH composite measured at various discharge current.

surface area of the sample calculated from N_2 desorption is 792 m^2/g. From the above results, we believe that the large surface area and porous hierarchical coating structure can really enhance the electrochemistry property of Fe_3O_4, which makes potential use for modification of other metal oxides as supercapacitor.

3.2. Electrochemical properties

For exploring the potential application in high performance supercapacitor of Fe_3O_4@C@Ni-Al LDH microspheres, the CV curves with various scan rates between 5 and 50 mV s^{-1} are measured in 6 M KOH aqueous electrolyte. As shown in Fig. 6A, it is obvious that the current response shows corresponding increases with the increasing of the scan rate, indicating a good capacitive behaviour of the electrode which can be ascribed to the facile iondiffusion and good adsorption properties. The shape of the CV curves is not significantly influenced by the increase of the scan rate from 5 and 50 mV s^{-1} which should result from the improved mass transportation and electron conduction. Moreover, the anodic peaks shift toward positive potential and the cathode peaks shift toward negative potential due to the electrode polarization at larger scan rates, which demonstrate the good electrochemical reversibility and high power character of Fe_3O_4@C@Ni-Al LDH microspheres.[43,47] Galvanostatic charging–discharging is a complementary method for measuring the specific capacitance of electrochemical capacitors at constant current. Plot of voltage versus time for this modificatorysupercapacitor at various current densities (1, 2, 3, 5, 8, 10 A/g) is shown in Fig 6B. The discharge time decreases monotonically with the increasing current density, resulting in the kinetics of the redox reacting progressively to sluggish to keep pace with fast potential change. The specific capacitance can be calculated from the following equation:

$$C_{sp} = \frac{I \times t}{V \times m} \quad (1)$$

Where C_{sp} is the specific capacitance (F/g), I is the discharge current (A), t is the discharge time (s), V is the potential range during discharge (V), and m is the mass of the active material in the electrode. According to the equation, the specific capacitance of the composite can be calculated based on the discharge curves (Fig. 7B) and typical data is shown in Fig. 7C for comparison. In order to further stress the electrochemical capacitive performance of the Fe_3O_4@C@Ni-Al LDH microspheres, cyclic voltammetry and galvanostatic charge-discharge have been carried out at potential intervals from 0–0.37 V in 6 M KOH aqueous electrolyte. To compare the electrochemical performance of the products, Fig. 7A illustrates the CV curves for the products at the scan rate of 5 mV/s. It can be seen that the CV curve of pure Fe_3O_4 microsphere displays the pair of cathodic and anodic peaks, which is associated with the reversible reaction of Fe (II) ↔ Fe (III). Compared with pure Fe_3O_4, both the internal area and the peak intensity of CV curve for Fe_3O_4/C spheres are apparently increased, implying that the specific capacitance of Fe_3O_4@C spheres is higher than that of pure Fe_3O_4. Furthermore, Fe_3O_4@C spheres have wider separation between anodic peak and cathodic peak, suggesting better electrochemical reaction reversibility. After surface modification of LDH coating was employed towards pure Fe_3O_4, the CV curve consists of a pair of redox peaks, corresponding to the plausible redox of Ni^{2+}/Ni^{3+} associated with OH^-, which can clearly reveal that the capacitance of the material mainly results from contribution of Faradic preudocapacitor.[45] From Fig 7A, we can see that the CV patterns of Fe_3O_4@C@Ni-Al LDH with largest separation between level anodic and cathodic currents combined together to form a single intense anodic peak which is attributed to the synergistic effect among these three components mentioned above. Since the specific capacitance is proportional to the area surrounded by the CV curves, the area under the CV curves for the Fe_3O_4@C@Ni-Al LDH is much higher than those of other composites at the same scan rate, indicating high capacitance. In the Fe_3O_4@C@Ni-Al LDH composite, the conductive material

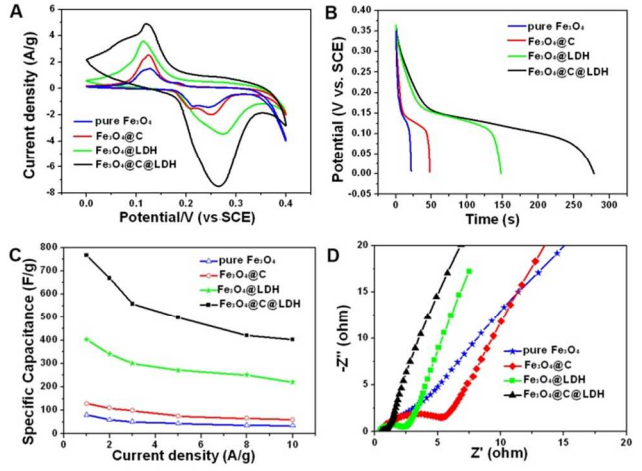

Fig. 7 Cyclic voltammograms (CVs) curves (A); galvanostatic (GV) discharge curves (B); current density dependence of the specific capacitance(C); Nyquist plots of the EIS for pure Fe_3O_4, Fe_3O_4@C, Fe_3O_4@Ni-Al LDH and Fe_3O_4@C@Ni-Al LDH composite (D).

Fe_3O_4 spheres are encapsulated in carbon layer and LDH, which can not only improve the electron conductivity of the anodes but thus increase the surface area to provide better access for electrolyte into the entire structure.

The specific capacitance of each sample is further confirmed by discharge curves at a current density of 1 A/g within a potential range 0 to 0.37 V in Fig. 7B. As shown, the discharge curves are not ideal straight lines and exhibit tow different sections, a fast potential drop followed by a slow potential drop, which also suggests the Faradic reaction is proceeding. The corresponding specific capacitance is 767.6, 405.4, 128.5, 78.7 F/g at a current density of 1 A/g for Fe_3O_4@C@Ni-Al LDH, Fe_3O_4@Ni-Al LDH, Fe_3O_4@C, and Fe_3O_4, respectively (on the basis of eq 1), which is consistent with the result of CVs that Fe_3O_4@C@Ni-Al LDH has the highest specific capacitance. Obviously, carbon coating and LDH modification can collaboratively enhance the capacitive performance of the metal oxide.

Good rate performance is a key requirement for evaluating the power application of supercapacitors.[59,60] As shown in Fig. 7C, the specific capacitances of the four samples were measured at different current densities (1, 2, 3, 5, 8, 10 A/g) for comparison purpose. Similarly, all specific capacitances of Fe_3O_4@C@Ni-Al LDH electrode are higher than those of other samples. The enhancement in specific capacitance can be attributed to the unique properties of carbon layer and the coating LDH. On one hand, those two layers can act as efficient electrically conductive networks. On other hand, these two materials can provide electrochemical capacitance, which results in synergistic effect between modificatory materials and Fe_3O_4. The maximum specific capacitance for the ternary-component composites reaches 767.6 F/g at 1 A/g, and maintains at 406 F/g when the scan rate is up to 10 A/g, indicating that the composite has a good rate capability, which is crucial for the electrode materials or supercapacitors to achieve both high power and energy densities.

The enhanced electrochemical performance of the Fe_3O_4@C@Ni-Al LDH microsphere was further confirmed by the electrochemical impedance spectroscopy (EIS) measurements to reveal the conductivity of the samples. The EIS data for pure Fe_3O_4, Fe_3O_4@C, Fe_3O_4@Ni-Al LDH, and Fe_3O_4@C@Ni-Al LDH were analyzed by Nyquist as shown in Fig. 7D. For each electrode, its Nyquist plot consists of a semicircle in high-frequency region followed by a straight line along the imaginary axis in the low frequency region. It is well accepted that the semicircle diameter of EIS equals to the electrochemical reaction impedance of the electrode, and the straight line indicates the diffusion of the electroactive species. A bigger semicircle means a larger charge transfer resistance, and a higher slope reflects a lower diffusion rate.[61,62] Notably, we can observe from the figure that Fe_3O_4@C@Ni-Al LDH contains a much smaller semicircle and a smaller slope, corresponding to a smaller charge transfer resistance (R_f) and ion diffusion resistance, which results in the higher reactivity and faster reaction kinetics.[63] This is probably due to the higher specific surface area of carbon and Ni-Al LDH layers, which facilitates the effective exposure of active sites.[43]

The durability of Fe_3O_4@C@Ni-Al LDH as the electrode material of supercapacitor was examined by specific capacitance at different cycles. Fig. 8 shows the cyclic performance of the

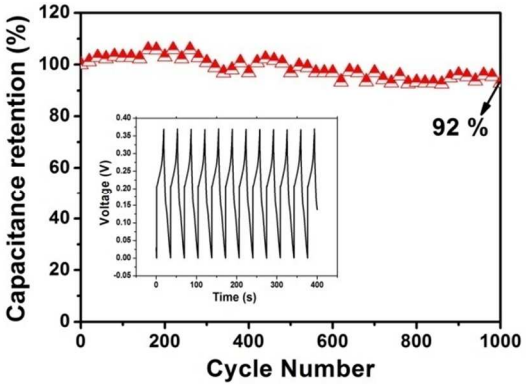

Fig. 8 Cycling performance of Fe_3O_4@C@Ni-Al LDH composite measured at 8 A/g with a voltage window of 0–0.37 V.

Fe_3O_4@C@Ni-Al LDH electrode carried out by galvanostatic charge-discharge tests at a current density of 8 A/g in the potential window from 0 to 0.37 V for 1000 cycles. During the first 300 cycles, the specific capacitance is increased by about 7%, which may be ascribed to the active materials which could be activated to produce available active sites and allows the trapped ions to gradually diffuse out at the initial stage. After 1000 cycles, the Fe_3O_4@C@Ni-Al LDH electrode exhibits excellent cycle stability, which has only 8% decrease of the initial available capacitance. The excellent cycling stability of the composite is attributable to the network of the special porous structure of Ni-Al LDH on Fe_3O_4, which effectively forms an open structure to improve the connection between the active materials during charge-discharge cycles, inhibits the capacitance loss, and exploits the full advantages of Fe_3O_4 electrode.[64,65] Moreover, carbon layer after annealing treatment in Ar has a good electrical conductivity and serves as a conductive matrix to provide a conductive network for electron transport during the electrode reaction process, which is favourable for stabilizing the electronic and ionic conductivities, therefore leading to a higher specific capacity and life-cycle durability.

4. Conclusions

In summary, we have developed a new strategy to prepare Fe_3O_4@C@Ni-Al LDH composite by a combination of the hydrothermal method and a facile *in situ* growth process. When was employed as supercapacitor electrodes, the Fe_3O_4@C@Ni-Al LDH composite displayed much higher specific capacitance, superior capacitance retention upon cycling, lower charge-transfer resistance and ion diffusion resistance than that of either pure Fe_3O_4 or pure Fe_3O_4 coated single layer. The composite electrode exhibits the specific capacitance as high as 767.6 F/g at 1A/g in 6 M KOH solution. This composite also shows stable cycling performance with slight decrease in the specific capacitance after 1000 charge/discharge cycles. This novel synthetic route towards metal hydroxide is of highly potential for supercapacitor due to largely enhanced electrochemical property.

Acknowledgements

Financial supports from the National Natural Science Foundation of China (NSFC 21271053), Research Fund for the Doctoral Program of Higher Education of China (20112304110021),

Natural Science Foundation of Heilongjiang Province (LC2012C10), Program for New Century Excellent Talents in University, Harbin Sci.-Tech. Innovation Foundation (RC2012XK017012), and the Fundamental Research Funds for the Central Universities of China are greatly acknowledged.

Notes and references

Key Laboratory of Superlight Materials and Surface Technology, Ministry of Education, College of Material Science and Chemical Engineering, Harbin Engineering University, Harbin 150001, P. R. China. E-mail: yangpiaoping@hrbeu.edu.cn; lirumin@hrbeu.edu.cn

1 L. Zhou, D. Y. Zhao and X. W. Lou, *Angew. Chem. Int. Ed.*, 2012, **51**, 239.
2 P. Simon and Y. Gogotsi, *Nat. Mater.*, 2008, **7**, 845.
3 Y. Wang, Z. Q. Shi, Y. Huang, Y. F. Ma, C. Y. Wang, M. M. Chen and Y. S. Chen, *J. Phys. Chem. C*, 2009, **113**, 13103.
4 L. L. Zhang and X. S. Zhao, *Chem. Soc. Rev.*, 2009, **38**, 2520.
5 Y. W. Zhu, S. Murali, M. D. Stoller, K. J. Ganesh, W. W. Cai, P. J. Ferreira, A. Pirkle, R. M. Wallace, K. A. Cychosz, M. Thommes, D. Su, E. A. Stach and R. S. Ruoff, *Science*, 2011, **332**, 1537.
6 X. W. Lou, J. S. Chen, P. Chen and L. A. Archer, *Chem. Mater.*, 2009, **21**, 2868.
7 M. Xu, L. Kong, W. Zhou and H. Li, *J. Phys. Chem. C*, 2007, **111**, 19141.
8 C. Z. Yuan, X. G. Zhang, L. H. Su, B. Gao and L. F. Shen, *J. Mater. Chem.*, 2009, **19**, 5772.
9 T. Brousse, P. L. Taberna, O. Crosnier, R. Dugas, P. Guillemet, Y. Scudeller, Y. Zhou, F. Favier, D. Belanger and P. Simon, *J. Power Sources*, 2007, **173**, 633.
10 V. Subramanian, H. W. Zhu and B. Q. Wei, *Electrochem. Commun.*, 2006, **8**, 827.
11 G. W. Yang, C. L. Xu and H. L. Li, *Chem. Commun.*, 2008, **48**, 6537.
12 Z. S. Wu, D. W. Wang, W. Ren, J. Zhao, G. Zhou, F. Li and H. M. Cheng, *Adv. Funct. Mater.*, 2010, **20**, 3595.
13 X. H. Xia, J. P. Tu, Y. J. Mai, X. L. Wang, C. D. Gu and X. B. Zhao, *J. Mater. Chem.*, 2011, **21**, 9319.
14 J. W. Xiao and S. H. Yang, *J. Mater. Chem.*, 2012, **22**, 12253.
15 B. Djurfors, J. N. Broughton, M. J. Brett and D. G. Ivey, *Acta Mater.*, 2005, **53**, 957.
16 N. Du, H. Zhang, B. Chen, J. B. Wu, X. Y. Ma, Z. H. Liu, Y. Q. Zhang, D. Yang, X. H. Huang and J. P. Tu, *Adv. Mater.*, 2007, **19**, 4505.
17 L. Wang, H. Ji, S. Wang, L. Kong, X. Jiang and G. Yang, *Nanoscale*, 2013, **5**, 3793.
18 X. Zhao, C. Johnston, A. Crossley and P. S. Grant, *J. Mater. Chem.*, 2010, **20**, 7637.
19 J. X. Zhu, Z. Y. Yin, D. Yang, T. Sun, H. Yu, H. E. Hoster, H. H. Hng, H. Zhang and Q. Y. Yan, *Enery Environ Sci.*, 2013, **6**, 987.
20 R. Li, X. Ren, F. Zhang, C. Du and J. Liu, *Chem. Commun.*, 2012, **48**, 5010.
21 L. Wang, T. Fei, Z. Lou and T. Zhang, *ACS Appl. Mat. Interfaces*, 2011, **3**, 4689.
22 W.-M. Zhang, X.-L. Wu, J.-S. Hu, Y.-G. Guo and L.-J. Wan, *Adv. Funct. Mater.*, 2008, **18**, 3941.
23 L. Wu, H. Yao, B. Hu and S.-H. Yu, *Chem. Mater.*, 2011, **23**, 3946.
24 Z. G. Wang, G. Cheng, Y. L. Liu, J. L. Zhang, D. H. Sun and J. Z. Ni, *J. Mater. Chem. B.*, 2013, **1**, 4845.
25 Z. Ren, Y. B. Guo, G. Wrobel, D. A. Knecht, Z. H. Zhang, H. Y. Gao and P. X. Gao, *J. Mater. Chem.*, 2012, **22**, 6862.
26 S. H. Xuan, F. Wang, X. L. Gong, S. K. Kong, J. C. Yu and K. C. F. Leung, *Chem. Commun.*, 2011, **47**, 2514.
27 S. Y. Wang, K. C. Ho, S. L. Kuo and N. L. Wu, *J. Electrochem. Soc.*, 2006, **153**, 75.
28 W. Li, Y. H. Deng, Z. X. Wu, X. F. Qian, J. P. Yang, Y. Wang, D. Gu, F. Zhang, B. Tu and D. Y. Zhao, *J. Amer. Chem. Soc.*, 2011, **133**, 15830.
29 X. Du, C. Y. Wang, M. M. Chen, Y. Jiao and J. Wang, *J. Phys. Chem. C*, 2009, **113**, 2643.
30 W. H. Shi, J. X. Zhu, D. H. Sim, Y. Y. Tay, Z. Y. Lu, X. J. Zhang, Y. Sharma, M. Srinivasan, H. Zhang, H. H. Hng and Q. Y. Yan, *J. Mater. Chem.*, 2011, **21**, 3422.
31 Q. Wang, L. Jiao, H. Du, Y. Wang and H. Yuan, *J. Power Sources*, 2014, **245**, 101.
32 J. Mu, B. Chen, Z. Guo, M. Zhang, Z. Zhang, P. Zhang, C. Shao and Y. Liu, *Nanoscale*, 2011, **3**, 5034.
33 G. P. Wang, L. Zhang and J. J. Zhang, *Chem. Soc. Rev.*, 2012, **41**, 797.
34 E. Frackowiak, V. Khomenko, K. Jurewicz, K. Lota and F. Beguin, *J. Power Sources*, 2006, **153**, 413.
35 T. Sato, G. Masuda and K. Takagi, *Electrochim. Acta*, 2004, **49**, 3603.
36 W. Xing, S. Z. Qiao, R. G. Ding, F. Li, G. Q. Lu, Z. F. Yan and H. M. Cheng, *Carbon*, 2006, **44**, 216.
37 J. P. Liu, J. Jiang, C. W. Cheng, H. X. Li, J. X. Zhang, H. Gong and H. J. Fan, *Adv. Mater.*, 2011, **23**, 2076.
38 H. Tang, J. H. Chen, Z. P. Huang, D. Z. Wang, Z. F. Ren, L. H. Nie, Y. F. Kuang and S. Z. Yao, *Carbon*, 2004, **42**, 191.
39 C. Nethravathi, C. R. Rajamathi, M. Rajamathi, R. Maki, T. Mori, D. Golberg and Y. Bando, *J. Mater. Chem. A.*, 2014, **2**, 985.
40 X. F. Zhang, J. Wang, R. M. Li, Q. H. Dai, R. Gao, Q. Liu and M. L. Zhang, *Ind. Eng. Chem. Res.*, 2013, **52**, 10152.
41 M. Shao, F. Ning, J. Zhao, M. Wei, D. G. Evans and X. Duan, *J. Am. Chem. Soc.*, 2012, **134**, 1071.
42 F. Leroux, A. Illaik, T. Stimpfling, A. L. Troutier-Thuilliez, S. Fleutot, H. Martinez, J. Cellier and V. Verney, *J. Mater. Chem.*, 2010, **20**, 9484.
43 A. Malak-Polaczyk, C. Vix-Guterl and E. Frackowiak, *Energy Fuels*, 2010, **24**, 3346.
44 L. Wang, D. Wang, X. Y. Dong, Z. J. Zhang, X. F. Pei, X. J. Chen, B. A. Chen and J. A. Jin, *Chem. Commun.*, 2011, **47**, 3556.
45 M. Shao, F. Ning, Y. Zhao, J. Zhao, M. Wei, D. G. Evans and X. Duan, *Chem. Mater.*, 2012, **24**, 1192.
46 W. Yang, Z. Gao, J. Wang, J. Ma, M. Zhang and L. Liu, *ACS Appl. Mat. Interfaces*, 2013, **5**, 5443.
47 B. Wang, Q. Liu, Z. Y. Qian, X. F. Zhang, J. Wang, Z. S. Li, H. J. Yan, Z. Gao, F. B. Zhao and L. H. Liu, *J. Power Sources*, 2014, **246**, 747.
48 J. Liu, Y. Li, X. Huang, G. Li and Z. Li, *Adv. Funct. Mater.*, 2008, **18**, 1448.
49 L. Zhang, J. Wang, J. Zhu, X. Zhang, K. San Hui and K. N. Hui, *J. Mater. Chem. A*, 2013, **1**, 9046.
50 C. Nethravathi, A. A. Jeffery, M. Rajamathi, N. Kawamoto, R.Tenne, D. Golberg and Y. Bando, *ACS Nano*, 2013, **7**, 7311.
51 X. Wang, A. Sumboja, M. Lin, J. Yan and P. S. Lee, *Nanoscale*, 2012, **4**, 7266.
52 F. Zhang, T. Zhang, X. Yang, L. Zhang, K. Leng, Y. Huang and Y. Chen, *Energy Environ. Sci.*, 2013, **6**, 1623.
53 M. E. Plonska-Brzezinska, D. M. Brus, A. Molina-Ontoria and L. Echegoyen, *RSC Adv.*, 2013, **3**, 25891.
54 M. Q. Zhao, Q. Zhang, J. Q. Huang, G. L. Tian, T. C. Chen, W. Z. Qian and F. Wei, *Carbon*, 2013, **54**, 403.
55 T. Stimpfling and F. Leroux, *Chem. Mater.*, 2010, **22**, 974.
56 L. Huang, D. C. Chen, Y. Ding, S. Feng, Z. L. Wang and M. L. Liu, *Nano Lett.*, 2013, **13**, 3135.
57 H. Y. Mi, X. G. Zhang, X. G. Ye and S. D. Yang, *J. Power Sources*, 2008, **176**, 403.
58 P. Yang, Z. Quan, Z. Hou, C. Li, X. Kang, Z. Cheng and J. Lin, *Biomaterials*, 2009, **30**, 4786.
59 A. C. Ferrari, J.C. Meyer, V. Scardaci, C. Casiraghi, M. Lazzeri, F. Mauri, S. Piscanec, D. Jiang, K. S. Novoselov, S. Roth, A. K. Geim, *Phys. Rev. Lett.*, 2006, **97**, 187401.
60 X. J. Zhang, W. H. Shi, J. X. Zhu, W. Y. Zhao, J. Ma, S. Mhaisalkar, T. L.Maria, Y. H. Yang, H. Zhang, H. H. Hng, Q. Y. Yan, *Nano Res.*, 2010, **3**, 643.
61 Y. Wang, S. L. Gai, N. Niu, F. He and P. P. Yang, *J. Mater. Chem. A.*, 2013, **1**, 9083.
62 R. Ding, L. Qi, M. J. Jia and H. Y. Wang, *J. Power Sources*, 2014, **251**, 287.
63 H. L. Wang, H. S. Casalongue, Y. Y. Liang and H. J. Dai, *J. Amer. Chem. Soc.*, 2010, **132**, 7472.
64 J. Xu, S. L. Gai, F. He, N. Niu, P. Gao, Y. J. Chen and P. P. Yang, *J.*

Mater. Chem. A., 2014, **2**, 1022.
65 J. P. Cheng, J. H. Fang, M. Li, W. F. Zhang, F. Liu and X. B. Zhang, *Electrochim. Acta*, 2013, **114**, 68.

A novel core-shell structured Fe_3O_4@C@Ni-Al LDH microspheres were prepared by a hydrothermal method followed a facile *in situ* growth process. The as-prepared product exhibits high pseudo-capacitor (767.6 F/g), good rate capability, and remarkable cycling stability (92% after 1000 cycling).